Proc. R. Soc. Lond. A **417**, 59–80 (1988)
Printed in Great Britain

Bounds on the conductivity of a random array of cylinders

BY S. TORQUATO[1] AND F. LADO[2]

[1] *Departments of Mechanical and Aerospace Engineering and of Chemical Engineering, North Carolina State University, Raleigh, North Carolina* 27695–7910, *U.S.A.*

[2] *Department of Physics, North Carolina State University, Raleigh, North Carolina* 27695-8202, *U.S.A.*

(*Communicated by M. E. Fisher, F.R.S.* – *Received* 30 *June* 1987 – *Revised* 10 *September* 1987)

We consider the problem of determining rigorous third-order and fourth-order bounds on the effective conductivity σ_e of a composite material composed of aligned, infinitely long, equisized, rigid, circular cylinders of conductivity σ_2 randomly distributed throughout a matrix of conductivity σ_1. Both bounds involve the microstructural parameter ζ_2 which is an integral that depends upon S_3, the three-point probability function of the composite (G. W. Milton, *J. Mech. Phys. Solids* **30**, 177–191 (1982)). The key multidimensional integral ζ_2 is greatly simplified by expanding the orientation-dependent terms of its integrand in Chebyshev polynomials and using the orthogonality properties of this basis set. The resulting simplified expression is computed for an equilibrium distribution of rigid cylinders at selected ϕ_2 (cylinder volume fraction) values in the range $0 \leqslant \phi_2 \leqslant 0.65$. The physical significance of the parameter ζ_2 for general microstructures is briefly discussed. For a wide range of ϕ_2 and $\alpha \doteq \sigma_2/\sigma_1$, the third-order bounds significantly improve upon second-order bounds which only incorporate volume fraction information; the fourth-order bounds, in turn, are always more restrictive than the third-order bounds. The fourth-order bounds on σ_e are found to be sharp enough to yield good estimates of σ_e for a wide range of ϕ_2, even when the phase conductivities differ by as much as two orders of magnitude. When the cylinders are perfectly conducting ($\alpha = \infty$), moreover, the fourth-order lower bound on σ_e provides an excellent estimate of this quantity for the entire volume-fraction range studied here, i.e. up to a volume fraction of 65%.

1. INTRODUCTION

This paper studies the problem of predicting the effective thermal (or electrical) conductivity σ_e of a two-phase material composed of equisized, parallel, circular cylinders, of conductivity σ_2 and volume fraction ϕ_2, distributed randomly throughout a matrix of conductivity σ_1 and volume fraction ϕ_1. To determine σ_e exactly, it is necessary to know not only σ_1, σ_2 and $\phi_1 = 1-\phi_2$, but an infinite set of correlation functions which statistically characterize the microstructure of the two-phase medium (Brown 1955; Milton 1981; Torquato 1985*a*). Such a complete statistical characterization of the medium is almost never known in

practice. Given σ_1, σ_2, and limited microstructural information on the composite, one may rigorously bound σ_e, however. Rigorous upper and lower bounds on effective properties are useful because: (i) they enable one to test the merits of a theory or computer-simulation experiment for the property; (ii) as successively more microstructural information is included, the bounds become progressively tighter; (iii) one of the bounds can typically provide a relatively accurate estimate of the bulk property even when the reciprocal bound diverges from it (Torquato 1985*a*).

Using only σ_1, σ_2, and ϕ_2, Hashin (1970) has obtained the best possible bound on the effective conductivity of transversely isotropic fibre-reinforced materials. By a 'fibre-reinforced' material, we generically mean any material whose phase boundaries are cylindrical surfaces, with generators parallel to one axis.

More restrictive bounds which include additional microstructural information on the fibre-reinforced material have been derived by Silnutzer (1972) and Milton (1981) for any isotropic two-phase material. The Silnutzer bounds depend upon an integral ζ_2 which involves the three-point probability function S_3. $S_n(\boldsymbol{r}_1, \ldots, \boldsymbol{r}_n)$ gives the probability of finding n points at positions $\boldsymbol{r}_1, \ldots, \boldsymbol{r}_n$ all in one of the phases, say phase 2. Milton's bounds depend not only on ζ_2 but an integral involving S_4, which itself can be expressed solely in terms of ϕ_2 and ζ_2. Thus, the key microstructural parameter that arises in both the Silnutzer and Milton bound is ζ_2. Application of the Silnutzer and Milton bounds has been very limited because of the difficulty involved in ascertaining S_3, either experimentally or theoretically. Recently, Torquato & Stell (1982) have provided a means of systematically representing and calculating the S_n for random distributions of inclusions or particles, given the n-particle probability density function ρ_n which characterizes the probability of finding any n particles with a particular configuration.

To our knowledge, the Silnutzer and Milton bounds on σ_e have heretofore not been computed for the practically useful model of aligned, infinitely long, equisized, rigid, circular cylinders (or circular discs in two dimensions) distributed randomly throughout a matrix. In this study, we shall carry out such calculations. Using the series representation of the S_n for a distribution of identical discs (Torquato & Stell 1982), we first greatly simplify the key multidimensional cluster integral ζ_2 by expanding orientation-dependent terms of its integrand in Chebyshev polynomials and using the orthogonality properties of this basis set. This analysis is general in that it may be applied to composites consisting of inclusions of arbitrary shape, size and penetrability (e.g. rigid, circular cylinders with particle-size distributions; rigid, elliptical cylinders; partially penetrable cylinders). We then compute the microstructural parameter ζ_2 for an equilibrium distribution of cylinders (discs) from the well-known results for the structure of rigid-disc fluids (Lado 1968). We briefly discuss the physical significance of ζ_2 for general microstructures. The Silnutzer and Milton bounds are then evaluated for our model for a wide range of phase conductivities and volume fractions.

The rigid-disc model described above is a realistic model of fibre-reinforced materials possessing long but aligned impenetrable fibres. The results of this investigation are also of interest in thin-film physics, where films consisting of columns of one material in a matrix of another are observed (Perrins *et al.* 1979).

For reasons of mathematical analogy, the results of this study translate immediately into equivalent results for the dielectric constant and magnetic permeability of the composite, or the diffusion coefficient associated with flow past fixed inclusions.

2. Third-order and fourth-order bounds

Given σ_1, σ_2, ϕ_2, and two integrals involving certain three-point correlation functions, rigorous bounds on the effective conductivity σ_e of any fibre-reinforced material, statistically isotropic in the transverse plane, have been derived by Silnutzer (1972). Milton (1982) showed that the Silnutzer bounds may be expressed in terms of σ_1, σ_2, ϕ_2, and a single integral ζ_2 (defined below) which depends upon the three-point probability function described in the Introduction. The simplified form of the Silnutzer bounds are given by

$$\sigma_L^{(3)} \leqslant \sigma_e \leqslant \sigma_U^{(3)}, \tag{2.1}$$

where

$$\sigma_U^{(3)} = \left[\langle\sigma\rangle - \frac{\phi_1\phi_2(\sigma_2-\sigma_1)^2}{\langle\tilde{\sigma}\rangle + \langle\sigma\rangle_\zeta}\right] \tag{2.2}$$

and

$$\sigma_L^{(3)} = \left[\langle 1/\sigma\rangle - \frac{\phi_1\phi_2(1/\sigma_2-1/\sigma_1)^2}{\langle 1/\tilde{\sigma}\rangle + \langle 1/\sigma\rangle_\zeta}\right]^{-1}. \tag{2.3}$$

Here we define $\langle b\rangle = b_1\phi_1 + b_2\phi_2$, $\langle\tilde{b}\rangle = b_1\phi_2 + b_2\phi_1$, and $\langle b\rangle_\zeta = b_1\zeta_1 + b_2\zeta_2$, where b represents any property. In addition, we have

$$\zeta_2 = 1-\zeta_1 = \frac{2}{\pi\phi_1\phi_2} I[\hat{S}_3(r,s,t)], \tag{2.4}$$

$$\hat{S}_3(r,s,t) = S_3(r,s,t) - S_2(r)\,S_2(s)/S_1, \tag{2.5}$$

where I is an integral operator defined below. The quantities $S_2(r)$ and $S_3(r,s,t)$ are, respectively, the probabilities of finding in phase 2 the end points of a line segment of length r and the vertices of a triangle with sides of length r, s, and t. S_1 is simply the volume fraction ϕ_2 of phase 2.

For any function $f(r,s,t)$, the integral operator I is defined through the relation

$$I[f] = \frac{1}{2\pi}\int \mathrm{d}\boldsymbol{r}\,\mathrm{d}\boldsymbol{s} f(r,s,t)\frac{\cos 2\theta}{r^2 s^2} = \int_0^\infty \frac{\mathrm{d}r}{r}\int_0^\infty \frac{\mathrm{d}s}{s}\int_0^{2\pi} \mathrm{d}\theta f(r,s,t)\cos 2\theta, \tag{2.6}$$

where θ is the included angle opposite the side of length t, so that $t^2 = r^2 + s^2 - 2rs\cos\theta$. In the first line of (2.6), the vector positions $\boldsymbol{r}$ and $\boldsymbol{s}$ are integrated over the entire infinite area. Note that for any function f that does not depend upon t, we have that $I[f(r,s)] = 0$. Thus, although the term $S_2(r)\,S_2(s)/S_1$ of (2.5) contributes nothing to I, its presence ensures the absolute convergence of the integral $I[\hat{S}_3]$, i.e. $\hat{S}_3(r,s,t)$ tends to zero when $r\to 0$, $s\to 0$, $r\to\infty$, or $s\to\infty$ (Brown 1955).

The bounds (2.1) are exact through third order in $(\sigma_2-\sigma_1)$ and hence are referred to as third-order bounds. The fact that ζ_2 (or ζ_1) lies in the interval $[0,1]$

implies that the Silnutzer bounds always improve upon the corresponding second-order bounds of Hashin (1970). The Hashin upper bound on σ_e for $\sigma_2 \geqslant \sigma_1$ is exactly realized by a two-phase material composed of 'composite' cylinders consisting of a core of conductivity σ_1 and radius R_c, surrounded by a concentric shell of conductivity σ_2 and radius R_0. The ratio $R_c^2/R_0^2 = \phi_1$ and thus the composite cylinders fill all space, implying there is a distribution in their size ranging to the infinitesimally small. For $\zeta_1 = 0$ or, equivalently, for $\zeta_2 = 1$, the third-order bounds (2.1) coincide and are equal to the Hashin upper bound for $\sigma_2 \geqslant \sigma_1$. Hence, $\zeta_1 = 0$ (or $\zeta_2 = 1$) for the singly coated composite cylinder assemblage (CCA) corresponding to the second-order upper bound. The Hashin lower bound on σ_e for $\sigma_2 \geqslant \sigma_1$ corresponds to the singly coated CCA but with phase 1 interchanged with phase 2. For $\zeta_2 = 0$ ($\zeta_1 = 1$), the third-order bounds (2.1) coincide and are equal to the Hashin lower bound for $\sigma_2 \geqslant \sigma_1$. Therefore, for the CCA corresponding to the second-order lower bound, $\zeta_2 = 0$ (or $\zeta_1 = 1$).

Milton (1981) has derived fourth-order bounds on σ_e, which depend not only upon σ_1, σ_2, and ζ_2, but upon a multifold integral that depends upon the four-point probability function S_4. (Note that these fourth-order bounds on σ_e are the two-dimensional analogues of bounds derived by Phan-Thien & Milton (1982) for three-dimensional isotropic two-phase composites.) Using a phase-interchange theorem for fibre-reinforced materials, Milton showed that the microstructural parameter involving S_4 can be expressed in terms of ϕ_2 and ζ_2 only. Milton's fourth-order bounds for transversely isotropic materials, for the case $\sigma_2 \geqslant \sigma_1$, are given by

$$\sigma_L^{(4)} \leqslant \sigma_e \leqslant \sigma_U^{(4)}, \tag{2.7}$$

where

$$\sigma_U^{(4)} = \sigma_2\left[\frac{(\sigma_1+\sigma_2)(\sigma_1+\langle\sigma\rangle)-\phi_2\zeta_1(\sigma_2-\sigma_1)^2}{(\sigma_1+\sigma_2)(\sigma_2+\langle\tilde{\sigma}\rangle)-\phi_2\zeta_1(\sigma_2-\sigma_1)^2}\right] \tag{2.8}$$

and

$$\sigma_L^{(4)} = \sigma_1\left[\frac{(\sigma_1+\sigma_2)(\sigma_2+\langle\sigma\rangle)-\phi_1\zeta_2(\sigma_2-\sigma_1)^2}{(\sigma_1+\sigma_2)(\sigma_1+\langle\tilde{\sigma}\rangle)-\phi_1\zeta_2(\sigma_2-\sigma_1)^2}\right]. \tag{2.9}$$

The upper bound (2.8) is exactly realized for a two-phase system composed of composite circular cylinders consisting of a core of conductivity σ_2 and radius R_c, surrounded by a concentric shell of conductivity σ_1 and outer radius R_0, which is in turn surrounded by a concentric shell of conductivity σ_2 and outer radius R. The ratio R_c^2/R_0^2 is such that it equals the product $\phi_1\zeta_1$ and the composite cylinders fill all space, implying that there is a distribution in their sizes ranging to the infinitesimally small. For this doubly coated CCA, the more conducting phase (phase 2) is generally the continuous phase and hence the CCA percolates for all ϕ_1, except $\phi_2 = 0$. This means that the fourth-order upper bound on σ_e goes to ∞ in the limit $\alpha = \sigma_2/\sigma_1 \to \infty$. (This statement applies as well to the second-order and third-order upper bounds.) The fourth-order lower bound (2.9) is realized for the aforementioned doubly coated CCA, but where the role of the individual phases are interchanged. Hence, the two-phase geometry corresponding to (2.9) generally possesses a dispersed or discontinuous conducting phase and can only percolate at the trivial value $\phi_2 = 1$. This implies that the fourth-order lower bound on σ_e always remains finite even in the limit $\alpha \to \infty$. (This statement applies as well to the second-order and third-order bounds.) Finally, we note that the Milton bounds

(2.7) always improve upon the second-order bounds of Hashin and the third-order bounds of Silnutzer.

The fact that the bounds diverge in the cases where the phase conductivities are drastically different does not mean the bounds have no use in such instances. Torquato (1985*a*) has observed that lower-order *lower* bounds (such as second-order, third-order, and fourth-order bounds) should yield good estimates of σ_e/σ_1 for $\alpha \gg 1$, provided that the volume fraction of the highly conducting phase, ϕ_2, is below its percolation-threshold value ϕ_2^c and that the average cluster size of phase 2, Λ_2, is much smaller than the scaled macroscopic dimension of the sample L. (A cluster of phase i is defined as that part of phase i which can be reached from a point in phase i without touching any part of phase j, $i \neq j$. L is defined to be the dimensional characteristic length of the sample divided by the microscopic lengthscale associated with inhomogeneities.) Of course, the accuracy of the lower-order lower bounds increases as the order increases. Note that the condition $\Lambda_2 \ll L$ alone implies that $\phi_2 < \phi_2^c$. For periodic as well as random arrays of impenetrable cylinders, the condition $\Lambda_2 \ll L$ is satisfied for all ϕ_2, except at the respective close-packing value, i.e. $\phi_2 = \phi_2^c$. Similarly, lower-order *upper* bounds on σ_e/σ_1 for $\alpha \gg 1$ should provide useful estimates of σ_e, given that $\phi_2 > \phi_2^c$ and $\Lambda_1 \ll L$, where Λ_1 is the average cluster size of phase 1. Again, the accuracy of the lower-order upper bounds increases as the order increases.

Until now, the three-point parameter ζ_2 has only been computed for two *random-media* models, namely, symmetric-cell materials (Beran & Silnutzer 1971) and fully penetrable cylinders (Torquato & Beasley 1986; Joslin & Stell 1986). Symmetric-cell materials (Miller 1969) are constructed by partitioning space into cells of possibly varying shapes and sizes, with cells randomly and independently designated as phase 1 or phase 2 with probabilities ϕ_1 and ϕ_2, respectively. Although a useful mathematical construct, a symmetric-cell material could not be used as a model of the more realistic two-phase microstructure of a distribution of equisized impenetrable cylinders in a matrix, because the space could not be completely filled by such cells. By 'fully penetrable' cylinders we mean a distribution of randomly centred, and thus spatially uncorrelated, cylinders. As the fibre fraction is increased for such distributions, the fibres tend to form clusters, and eventually, at the percolation threshold, changes from a discontinuous structure to a continuous one. The space ultimately can be entirely filled with cylinders. Hence, distributions of fully penetrable cylinders, at high fibre fractions, are not useful models of a large class of fibre-reinforced materials that possess impenetrable fibres. In many instances, the latter percolates or forms an infinite cluster only at the maximum, close-packing volume fraction of the system.

3. Simplification of the parameter ζ_2 for impenetrable cylinders

The general n-point probability function for the ith phase of a two-phase system of arbitrary dimensionality composed of inclusions distributed throughout a matrix phase has been shown by Torquato & Stell (1982) to be given by an infinite series. For the special case of an isotropic distribution of identical, impenetrable

discs (parallel cylinders) of radius R at area (volume) fraction ϕ_2, the infinite series for the probability function of the included phase (phase 2) terminates with the nth term (Torquato & Stell 1982). In the specific instance $n = 3$, it is given by

$$S_3(r_{12}, r_{13}, r_{23}) = S_3^{(1)}\phi_2 + S_3^{(2)}\phi_2^2 + S_3^{(3)}\phi_2^3, \tag{3.1}$$

where in the diagram notation of Torquato & Stell (1985).

$$S_3^{(1)} = \frac{1}{A_1}$$  (3.2)

$$S_3^{(2)} = \frac{1}{A_1^2}\Big[$$  $$\Big],$$ (3.3)

$$S_3^{(3)} = \frac{1}{A_1^3}$$  . (3.4)

In this shorthand, a solid circle represents a vector position that is integrated over the entire infinite area, the labelled open circles stand for $\boldsymbol{r}_1, \boldsymbol{r}_2$, or $\boldsymbol{r}_3$ (with $r_{ij} = |\boldsymbol{r}_j - \boldsymbol{r}_i|$), and the broken line represents the bond

$$m(r) = \begin{cases} 1, & r < R \\ 0, & r > R \end{cases} \tag{3.5}$$

between the two positions, the solid line represents the pair or radial distribution function g_2 of the discs, and the cross-hatched triangle for their triplet distribution function g_3; thus, for example,

 $= \int d\boldsymbol{r}_4\, d\boldsymbol{r}_5\, m(r_{14})\, m(r_{24})\, m(r_{35})\, g_2(r_{45}).$ (3.6)

The g_n are related to the n-particle probability density function ρ_n through $\rho_n = \rho^n g_n$, where ρ is the number density of discs (cylinders). Finally, $A_1 = \pi R^2$ is the area of one disc.

The graphs (3.2)–(3.4) have simple interpretations. $S_3^{(1)}\phi_2$ gives the contribution to S_3 when all three points lie in the same disc (or sphere in three dimensions): a quantity which is trivially related to the intersection area (volume) of three discs (spheres) with centres separated by distances r_{12}, r_{13}, and r_{23}. $S_3^{(2)}\phi_2^2$ is the probability of finding one point in one disc (sphere) and two points in some other disc (sphere). Finally, $S_3^{(3)}\phi_2^3$ gives the probability of finding each of the three points in different discs (spheres). Although $S_3^{(1)}$ is independent of ϕ_2, $S_3^{(2)}$ and $S_3^{(3)}$ are both functions of ϕ_2 through their dependence upon g_2 and g_3. Note that S_n in the papers by Torquato & Stell, unlike this work, denotes the probability function associated with the matrix phase, which actually is simply related to the included-phase counterpart (Torquato & Stell 1982).

It is seen that S_3 involves two-fold, four-fold, and six-fold integrals. Hence, the integral $I[\hat{S}_3]$ (and, thus, ζ_2) consists of complicated multifold integrals which we

now simplify. It should be noted that the analysis given below is general in that it may be applied to composites consisting of inclusions of arbitrary shape, size and penetrability (e.g. rigid, circular cylinders with particle-size distributions; rigid, elliptical cylinders; partly penetrable cylinders, etc.). The three-point probability function for dispersions containing particles of arbitrary shape and size has the same functional form as (3.1)–(3.4).

(*a*) *Evaluation of* $I[S_3^{(1)}]$

Keeping the origin of a polar coordinate system fixed at $\boldsymbol{r}_1$ and aligning the x-axis along $\hat{\boldsymbol{r}}_{12} = \boldsymbol{r}_{12}/r_{12}$ ($\boldsymbol{r}_{12} = \boldsymbol{r}_2 - \boldsymbol{r}_1$) for convenience, we have

$$= \int \mathrm{d}\boldsymbol{r}_4\, m(r_{14})\, m(r_{24})\, m(r_{34})$$

$$= \int_0^\infty \mathrm{d}r_{14}\, r_{14}\, m(r_{14}) \int_0^{2\pi} \mathrm{d}\theta_{214}\, m(r_{24})\, m(r_{34}), \tag{3.7}$$

where $\theta_{jik} \equiv \arccos(\hat{\boldsymbol{r}}_{ij} \cdot \hat{\boldsymbol{r}}_{ik})$.

The angular integration in (3.7) can be carried out by expanding the angle-dependent functions in a cosine series or equivalently in Chebyshev polynomials. For example,

$$m(r_{24}) = \sum_{n=0}^{\infty} M_n(r_{12}, r_{14})\, T_n(\cos\theta_{214}), \tag{3.8}$$

where $T_n(\cos\theta) = \cos n\theta$ is the Chebyshev polynomial of the first kind. The expansion coefficients are then given by

$$M_n(r_{12}, r_{14}) = \frac{c_n}{2\pi} \int_0^{2\pi} \mathrm{d}\theta_{214}\, m(r_{24})\, T_N(\cos\theta_{214}), \tag{3.9}$$

where

$$c_n = \begin{cases} 1, & n = 0, \\ 2, & n > 0. \end{cases} \tag{3.10}$$

In Appendix A it is shown that the coefficients may be alternatively expressed as

$$M_n(r_{12}, r_{14}) = \frac{c_n}{2\pi} \int_0^\infty \mathrm{d}k\, k\tilde{m}(k) J_n(kr_{14}) J_n(kr_{12}), \tag{3.11}$$

where $\tilde{m}(k)$ is the Fourier transform of $m(r)$ and $J_n(x)$ is the Bessel function of order n. Similarly, we write $m(r_{34})$ *as*

$$m(r_{34}) = \sum_{n=0}^{\infty} M_n(r_{13}, r_{14})\, T_n(\cos\theta_{314})$$

$$= \sum_{n=0}^{\infty} M_n(r_{13}, r_{14}) [T_n(\cos\theta_{214}) T_n(\cos\theta_{213}) + V_n(\cos\theta_{214})\, V_n(\cos\theta_{213})], \tag{3.12}$$

where, upon invoking the addition formula for the T_n (Abramowitz & Stegun 1964), we have introduced the Chebyshev polynomial $V_n(\cos\theta) = \sin n\theta$. The V_n are related to the Chebyshev polynomials of the second kind U_n defined in

Appendix B. The addition formula is used to bring out the specific angular variables needed. The orthogonality properties

$$\frac{1}{\pi}\int_0^{2\pi} d\theta\, T_m(x)\,T_n(x) = \begin{cases}\delta_{mn}, & m \neq 0\\ 2, & m = n = 0,\end{cases} \tag{3.13}$$

$$\frac{1}{\pi}\int_0^{2\pi} d\theta\, V_m(x)\,V_n(x) = \begin{cases}\delta_{mn}, & m \neq 0\\ 2, & m = n = 0,\end{cases} \tag{3.14}$$

$$\frac{1}{\pi}\int_0^{2\pi} d\theta\, V_m(x)\,T_n = 0, \quad \text{for all } m \text{ and } n, \tag{3.15}$$

will prove to be very useful. Here δ_{mn} is the Kronecker delta and $x = \cos\theta$.

Using the expansions (3.8) and (3.12), and the orthogonality relations (3.13)–(3.15), we now have in (3.7)

$$\int_0^{2\pi} d\theta_{214}\, m(r_{24})\, m(r_{34}) = \pi \sum_{n=0}^{\infty} c_n M_n(r_{12}, r_{14}) M_n(r_{13}, r_{14}) T_n(\cos\theta_{213}) \tag{3.16}$$

and thus finally

$$I\left[\begin{array}{c}\circ\\ \circ\quad\circ\\ 1\quad 2\quad 3\end{array}\right] = \int_0^{\infty}\frac{dr_{12}}{r_{13}}\int_0^{\infty}\frac{dr_{13}}{r_{13}}\int_0^{\infty} dr_{14}\, r_{14}\, m(r_{14})\int_0^{2\pi} d\theta_{213}$$

$$\times \pi \sum_{n=1}^{\infty} M_n(r_{12}, r_{14}) M_n(r_{13}, r_{14}) T_n(\cos\theta_{213}) T_2(\cos\theta_{213})$$

$$= \pi^2 \int_0^{\infty} dr\, r m(r)\left[\int_0^{\infty}\frac{ds}{s} M_2(r, s)\right]^2. \tag{3.17}$$

Now by (3.11) and noting that $\tilde{m}(k) = 2\pi R J_1(kR)/k$, we have

$$\int_0^{\infty}\frac{ds}{s} M_2(r, s) = 2R\int_0^{\infty} dk J_1(kR) J_2(kr)\int_0^{\infty} ds\frac{J_2(ks)}{s}$$

$$= \frac{R^2}{r^2} H(r-R), \tag{3.18}$$

where $H(x)$ is the Heaviside step function, defined to be zero when its argument is negative, one otherwise. (The Bessel function integrals used in getting (3.18) can be found in Abramowitz & Stegun (1964).) Because of the conflicting step functions, we finally find the simple result

$$I[S_3^{(1)}] = 0. \tag{3.19}$$

Because $S_3^{(1)}$ is independent of the structure, (3.19) is a universal result for any ensemble of equisized discs.

(*b*) *Evaluation of* $I[S_3^{(2)}]$

Again, keeping the origin of coordinates fixed at $\boldsymbol{r}_1$ and aligning the x-axis along $\hat{\boldsymbol{r}}_{12}$, the first graph of (3.3), with $m(r_{24})$, $m(r_{35})$ and $g_2(r_{45})$ expanded in Chebyshev polynomials, is given by

$$= \int_0^\infty \mathrm{d}r_{14}\, r_{14}\, m(r_{14}) \int_0^\infty \mathrm{d}r_{15}\, r_{15} \times \pi^2 \sum_{n=0}^{\infty} c_n^2 M_n(r_{12}, r_{14}) M_n(r_{13}, r_{15}) G_n(r_{14}, r_{15}) T_n(\cos\theta_{213}). \quad (3.20)$$

In arriving at (3.20) we again have used the addition formula for the T_n and the orthogonality properties of T_n and V_n. Here G_n are the expansion coefficients associated with the radial distribution function. Therefore,

$$I\left[\begin{array}{c}\bullet\!\!-\!\!\bullet \\ \circ\ \circ\ \circ \\ 1\ 2\ 3\end{array}\right] = \pi^3 R^4 \int_0^\infty \frac{\mathrm{d}r_{14}}{r_{14}} m(r_{14}) H(r_{14}-R) \int_0^\infty \frac{\mathrm{d}r_{15}}{r_{15}} G_2(r_{14}, r_{15}) H(r_{15}-R) = 0, \quad (3.21)$$

again because of the conflicting demands of the step functions on r_{14}. Interchanging the labels 2 and 3 clearly leads to the same integrals, thus the second diagram in (3.3) also contributes nothing to I.

The only non-zero contribution to I from (3.3) is from the last graph. Instead of integrating over $\boldsymbol{r}_2$, $\boldsymbol{r}_3$, $\boldsymbol{r}_4$, and $\boldsymbol{r}_5$, as we did for the two previous diagrams, we shall, by virtue of the homogeneity and isotropy of the system, integrate over $\boldsymbol{r}_1$, $\boldsymbol{r}_2$, $\boldsymbol{r}_3$, and $\boldsymbol{r}_4$. Hence, we have

$$I\left[\begin{array}{c}\dfrac{1}{A_1^2}\ \circ\!\!-\!\!\bullet \\ 2\ 3\ 1\end{array}\right] = \frac{1}{2\pi} \int \mathrm{d}\boldsymbol{r}_{45}\, g_2(r_{45})\, W(r_{45}), \quad (3.22)$$

where

$$W(r_{45}) = \frac{1}{A_1^2} \int \mathrm{d}\boldsymbol{r}_1\, \mathrm{d}\boldsymbol{r}_2\, \mathrm{d}\boldsymbol{r}_3\, m(r_{15})\ m(r_{24})\ m(r_{34}) \frac{T_2(\cos\theta_{213})}{r_{12}^2\, r_{13}^2}. \quad (3.23)$$

Now consider first the integral over $\boldsymbol{r}_3$ in (3.23) which requires the expansion of $m(r_{34})$ as in (3.12):

$$\int \mathrm{d}\boldsymbol{r}_3\, m(r_{34}) \frac{T_2(\cos\theta_{213})}{r_{13}^2} = \pi T_2(\cos\theta_{214}) \int_0^\infty \frac{\mathrm{d}r_{13}}{r_{13}} M_2(r_{13}, r_{14}) = A_1 H(r_{14}-R) \frac{T_2(\cos\theta_{214})}{r_{14}^2}. \quad (3.24)$$

The second line of (3.24) follows from (3.18). Because we have assumed the fibres (discs) to be mutually impenetrable, then the radial distribution function $g(r_{45}) = 0$ for $r_{45} < 2R$. Moreover, $m(r_{15}) = 0$ for $r_{15} > R$. Accordingly, for $r_{15} < R$ and $r_{45} > 2R$, we have $r_{14} > R$ and thus can drop the step function $H(r_{14}-R)$ from (3.24). In a similar manner, we get

$$\int \mathrm{d}\boldsymbol{r}_2\, m(r_{24}) \frac{T_2(\cos\theta_{214})}{r_{12}^2} = A_1 \frac{H(r_{14}-R)}{r_{14}^2}. \quad (3.25)$$

Application of (3.24) and (3.25) gives

$$W(r) = \int \mathrm{d}s \frac{m(s)}{t^4}$$

$$= \int_0^R \mathrm{d}s\, s \int_0^{2\pi} \frac{\mathrm{d}\theta}{(r^2+s^2-2rs\cos\theta)^2}$$

$$= \frac{A_1}{(r^2-R^2)^2}, \tag{3.26}$$

where $r \equiv r_{45}$, $s \equiv r_{15}$, $t \equiv r_{14}$, and θ is the angle opposite the triangle side of length t; the implied fixed origin is at $\boldsymbol{r}_5$ and the x-axis along $\hat{\boldsymbol{r}}_{45}$.

Introduction of (3.26) into (3.22) and use of (3.3) finally yields

$$I[S_3^{(2)}] = A_1 \int_{2R}^{\infty} \mathrm{d}r \frac{r g_2(r)}{(r^2-R^2)^2}, \tag{3.27}$$

where we have used the constraint that $g_2(r) = 0$ for $r < 2R$. Thus, we have reduced an eight-fold integral (3.22) to the one-dimensional quadrature (3.27).

(c) *Evaluation of* $I[S_3^{(3)}]$

Simplification of the final integral is again considerably aided by exploiting the freedom, offered by the homogeneity and isotropy of the system, to change as convenience dictates the origin and orientation of the coordinate frame. Consider writing the desired integral in the form

$$I[S_3^{(3)}] = \frac{1}{2\pi} \int \mathrm{d}\boldsymbol{r}_5\, \mathrm{d}\boldsymbol{r}_6\, g_3(r_{45}, r_{46}, r_{56})\, Q(r_{45}, r_{46}, r_{56}), \tag{3.28}$$

where

$$Q(r_{45}, r_{46}, r_{56}) = \frac{1}{A_1^3} \int \mathrm{d}\boldsymbol{r}_1\, \mathrm{d}\boldsymbol{r}_2\, \mathrm{d}\boldsymbol{r}_3\, m(r_{14})\, m(r_{25})\, m(r_{36}) \frac{T_2(\cos\theta_{213})}{r_{12}^2 r_{13}^2}. \tag{3.29}$$

The implied fixed origin for (3.28) is now at $\boldsymbol{r}_4$. Let us first consider the integral over $\boldsymbol{r}_3$ in (3.29), which requires expansion of $m(r_{36})$. With an origin of coordinates at $\boldsymbol{r}_1$ and the x-axis along $\hat{\boldsymbol{r}}_{12}$, we find

$$\int \mathrm{d}\boldsymbol{r}_3\, m(r_{36}) \frac{T_2(\cos\theta_{213})}{r_{13}^2} = A_1 \frac{H(r_{16}-R)}{r_{16}^2} T_2(\cos\theta_{216}). \tag{3.30}$$

The presence of the three-body distribution function g_3 in (3.28) requires $r_{46} > 2R$. This result combined with the constraint $r_{14} < R$ (because of $m(r_{14})$), necessarily gives that $r_{16} > R$ and hence we can drop the step function $H(r_{16}-R)$ in (3.30). Next consider the integral over r_2 such that we keep the origin at $\boldsymbol{r}_1$ but align the x-axis along $\hat{\boldsymbol{r}}_{16}$:

$$\int \mathrm{d}\boldsymbol{r}_2\, m(r_{25}) \frac{T_2(\cos\theta_{216})}{r_{12}^2} = A_1 \frac{H(r_{15}-R)}{r_{15}^2} T_2(\cos\theta_{516}). \tag{3.31}$$

As before, the step function $H(r_{15}-R)$ is always satisfied and hence (3.29) now becomes

$$Q(r_{45}, r_{46}, r_{56}) = \frac{1}{A_1}\int \mathrm{d}\boldsymbol{r}_1\, m(r_{14})\frac{T_2(\cos\theta_{516})}{r_{15}^2 r_{16}^2}. \tag{3.32}$$

Now to integrate over $\boldsymbol{r}_1$, we place the origin at $\boldsymbol{r}_4$. Because $\theta_{516} = \theta_{415}+\theta_{416}$, we have, using the addition formula for the T_n,

$$Q(r_{45}, r_{46}, r_{56}) = \frac{1}{A_1}\int_0^R \mathrm{d}r_{14}\, r_{14}\int_0^{2\pi}\mathrm{d}\theta_{146} \times\left[\frac{T_2(\cos\theta_{415})\,T_2(\cos\theta_{416}) - V_2(\cos\theta_{415})\,V_2(\cos\theta_{416})}{r_{15}^2 r_{16}^2}\right]. \tag{3.33}$$

It is shown in Appendix B that the expressions within the brackets in (3.33) can be expanded in terms of the corresponding opposite angles at the base of the coordinate frame, giving now

$$\begin{aligned} Q(r_{45}, r_{46}, r_{56}) &= \frac{1}{A_1}\int_0^R \mathrm{d}r_{14}\, r_{14}\int_0^{2\pi}\mathrm{d}\theta_{146} \\ &\quad\times \sum_{m,n=0}^{\infty}(m+1)(n+1)\frac{r_{14}^{m+n}}{r_{45}^{m+2}r_{46}^{n+2}}\left[T_{m+2}(\cos\theta_{145})\,T_{n+2}(\cos\theta_{146})\right. \\ &\quad\left. - V_{m+2}(\cos\theta_{145})\,V_{n+2}(\cos\theta_{146})\right] \\ &= \sum_{n=0}^{\infty}(n+1)\,R^{2n}\frac{T_{n+2}(\cos\theta_{546})}{r_{45}^{n+2}r_{46}^{n+2}}. \end{aligned} \tag{3.34}$$

The second line of (3.34) is obtained by applying the addition formulas to the $T_n(\cos\theta_{145})$ and $V_n(\cos\theta_{145})$ and then by using the orthogonality properties (3.13)–(3.15). Substitution of (3.34) into (3.28) yields

$$\begin{aligned} I[S_3^{(3)}] &= \frac{1}{2\pi}\sum_{n=0}^{\infty}(n+1)\,R^{2n}\int \mathrm{d}\boldsymbol{r}_5\,\mathrm{d}\boldsymbol{r}_6\, g_3(r_{45}, r_{46}, r_{56})\frac{T_{n+2}(\cos\theta_{546})}{r_{45}^{n+2}r_{46}^{n+2}} \\ &= 2\sum_{n=2}^{\infty}(n-1)\,R^{2n-4}\int_0^{\infty}\frac{\mathrm{d}r}{r^{n-1}}\int_0^{\infty}\frac{\mathrm{d}s}{s^{n-1}}\int_0^{\pi}\mathrm{d}\theta\, g_3(r,s,t)\,T_n(\cos\theta), \end{aligned} \tag{3.35}$$

where r, s, and t are the lengths of sides of a triangle and θ is the angle opposite the side of length t. Hence, we have reduced a tenfold integral (3.28) to the three-dimensional quadrature (3.35).

As remarked earlier, although the term $S_2(r)S_2(s)/S_1$ of (2.5) makes no contribution to I, its presence ensures the absolute convergence of the integral $I[\hat{S}_3]$. The expression for $S_2(r_{12})$ for the case of impenetrable discs can be obtained from (3.1)–(3.4) for $S_3(r_{12}, r_{13}, r_{23})$ by letting $\boldsymbol{r}_2 \to \boldsymbol{r}_3$:

$$S_2(r_{12}) = \left[\frac{1}{A_1}\right]\phi_2 + \left[\frac{1}{A_1^2}\right]\phi_2^2. \tag{3.36}$$

We can now summarize the results of this section for the simplification of (2.4) with the finding that, by (3.1), (3.19), (3.27), (3.35) and (3.36), we have

$$I[\hat{S}_3] = k_2\phi_2^2 + k_3\phi_2^3, \tag{3.37}$$

where

$$k_2 = \pi R^2 \int_{2R}^{\infty} \mathrm{d}r \frac{r g_2(r)}{(r^2-R^2)^2}, \tag{3.38}$$

$$k_3 = 4\sum_{n=2}^{\infty}(n-1)R^{2n-4}\int_0^{\infty}\frac{\mathrm{d}r}{r^{n-1}}\int_0^{r}\frac{\mathrm{d}s}{s^{n-1}}\int_0^{\pi}\mathrm{d}\theta\,[g_3(r,s,t)-g_2(r)g_2(s)]T_n(\cos\theta). \tag{3.39}$$

The term $g_2(r)g(s)$ in (3.39) arises from $I[S_2(r)S_2(s)/S_1]$ and hence ensures the convergence of k_3, a point of particular interest for numerical calculations. Note that the symmetry of the integrand in r and s has enabled us to change the limits of integration on s from $0 \leqslant s \leqslant \infty$ [(3.35)] to $0 \leqslant s \leqslant r$ [(3.39)]; this brings out a factor of two. The three-point parameter ζ_2 is trivially related to (3.37) through (2.4). It should be emphasized that (3.37)–(3.39) are valid for *any* isotropic distribution of equisized impenetrable cylinders.

4. Calculation of the three-point parameter ζ_2

Here we compute the microstructural parameter ζ_2 for a random distribution of parallel cylinders (discs) in a matrix. To evaluate the two-body and three-body integrals of (3.37) we need to know the pair g_2 and triplet g_3 distribution functions for the model. By assuming an equilibrium distribution of rigid cylinders, we can employ approximations for g_2 and g_3 used in the study of the liquid state. An equilibrium distribution of rigid discs may be regarded, in a qualitative sense, as the 'most' random distribution of discs subject to the constraint of mutual impenetrability. Specifically, we use the Percus–Yevick approximation to g_2 for rigid discs obtained numerically by Lado (1968). The calculation of the triplet distribution, as is well known, is more problematical. Lacking any more fundamental alternative, we turn to the familiar Kirkwood superposition approximation (Hansen & McDonald 1976).

$$g_3(r_{12}, r_{13}, r_{23}) \approx g_2(r_{12})\,g_2(r_{13})\,g_2(r_{23}), \tag{4.1}$$

to compute this quantity. The superposition approximation is exact for all possible configurations of three particles in the zero-density limit and when one particle is distant from the other two, regardless of the density. For equilateral-triangle configurations, the superposition approximation is accurate, especially at high densities; the approximation is less accurate at low densities and for less symmetric triplet configurations. A study by Beasley & Torquato (1986) indicates that the use of the superposition approximation to compute the three-dimensional analogue of ζ_2 for suspensions of spheres slightly underestimates the geometric parameter (i.e. provides a lower bound on ζ_2); the error increases with increasing density. The use of a lower bound on ζ_2 (at some fixed volume fraction) in either two-dimensional or three-dimensional conductivity bounds still provides rigorous bounds on σ_e, albeit bounds which are weaker than the ones incorporating the exact ζ_2. Because the integral (2.4) bears a strong similarity to its three-

dimensional counterpart, it is expected that application of the superposition approximation in (3.39) should not lead to significant errors in ζ_2. Henceforth, we shall denote g_2 by g.

For numerical calculations, it is advantageous to replace $g(r)$ in the first integral of (3.37) with $1+h(r)$, where $h(r)$ is the total correlation function. For cylinders of unit diameter, we have then

$$k_2 = \frac{\pi}{6}+\frac{\pi}{4}\int_1^\infty \mathrm{d}r \frac{rh(r)}{(r^2-\frac{1}{4})^2}, \tag{4.2}$$

where now the integrand with $h(r)$ vanishes rapidly for large r. Given the Percus–Yevick $h(r)$ (Lado 1968), the integral of (4.2) can be computed with any standard numerical quadrature technique.

In the superposition approximation, the second integral of (3.37) (for cylinders of unit diameter) becomes

$$k_3 = \sum_{n=2}^{\infty} \frac{n-1}{4^{n-3}} \int_1^\infty \mathrm{d}r \frac{g(r)}{r^{n-1}} \int_1^r \mathrm{d}s \frac{g(s)}{s^{n-1}} \int_0^\pi \mathrm{d}\theta\, h(t)\, T_n(\cos\theta). \tag{4.3}$$

Note that we have used the fact that $g(r) = 0$ for $r < 1$. We compute this threefold integral by using a Gaussian–Chebyshev quadrature technique (Abramowitz & Stegun 1964). Such numerical integration schemes have been used to accurately evaluate related multifold integrals (Torquato & Beasley 1986). Because $h(t) = -1$ for $t < 1$ and is discontinuous at $t = 1$, we rewrite the integral k_3 so as to explicitly account for the discontinuity at $t = 1$ and hence divide it up into the following five parts:

$$k_3 = \sum_{n=2}^{\infty} \frac{n-1}{4^{n-3}} [I_1+I_2+I_3+I_4+I_5], \tag{4.4}$$

where

$$I_1 = -\int_1^2 \mathrm{d}r \frac{g(r)}{r^{n-1}} \int_1^r \mathrm{d}s \frac{g(s)}{s^{n-1}} \int_0^{\theta_c} \mathrm{d}\theta\, T_n(\cos\theta), \tag{4.5}$$

$$I_2 = -\int_2^\infty \mathrm{d}r \frac{g(r)}{r^{n-1}} \int_{r-1}^r \mathrm{d}s \frac{g(s)}{s^{n-1}} \int_0^{\theta_c} \mathrm{d}\theta\, T_n(\cos\theta), \tag{4.6}$$

$$I_3 = \int_1^2 \mathrm{d}r \frac{g(r)}{r^{n-1}} \int_1^r \mathrm{d}s \frac{g(s)}{s^{n-1}} \int_{\theta_c}^\pi \mathrm{d}\theta\, h(t)\, T_n(\cos\theta), \tag{4.7}$$

$$I_4 = \int_2^\infty \mathrm{d}r \frac{g(r)}{r^{n-1}} \int_1^{r-1} \mathrm{d}s \frac{g(s)}{s^{n-1}} \int_0^\pi \mathrm{d}\theta\, h(t)\, T_n(\cos\theta), \tag{4.8}$$

$$I_5 = \int_2^\infty \mathrm{d}r \frac{g(r)}{r^{n-1}} \int_{r-1}^r \mathrm{d}s \frac{g(s)}{s^{n-1}} \int_{\theta_c}^\pi \mathrm{d}\theta\, h(t)\, T_n(\cos\theta). \tag{4.9}$$

In the equations above, $\theta_c = \arccos\,[(r^2+s^2-1)/2rs]$ is the angle at which $t = 1$. Equations (4.5) and (4.6) thus give the contribution to k_3 for $t < 1$. The remaining integrals, (4.7)–(4.9), give the contribution to k_3 for $t > 1$. To ensure proper sampling of the integration region, the integrals I_i were subdivided further so that 24 gaussian points in each dimension gave convergence to four significant figures. In principle, the expansion (4.4) in Chebyshev polynomials is infinite, but in

practice only the first seven to nine terms are needed to give convergence to four significant figures. To compute k_3 at large volume fractions (the most time-intensive cases), the gaussian quadrature scheme required about 48 min of CPU time on a VAX 785. We also evaluated the two-body integral of (4.2) using the same gaussian technique; here we used 64 gaussian points.

In table 1 we present our results for the microstructural parameter

$$\zeta_2 = \frac{2}{\pi\phi_1}[k_2\phi_2 + k_3\phi_2^2] \tag{4.10}$$

at selected values of the volume fraction. Because the Percus–Yevick approximation for the pair distribution function appears to break down as the random close-packing volume fraction $\phi_2 \approx 0.81$ (Stillinger *et al.* 1964) is approached, the highest volume fraction reported here is $\phi_2 = 0.65$, at which the Percus–Yevick results are still in relatively good agreement with Monte Carlo simulations. The percolation threshold ϕ_2^c for an equilibrium distribution of impenetrable discs has been conjectured to be the random-packing limit. The value $\phi_2 = 0.65$ is considerably above the close-packing volume fraction of 0.55 for random sequential addition of rigid discs (Feder 1980).

TABLE 1. THREE-POINT PARAMETER ζ_2 FOR AN EQUILIBRIUM DISTRIBUTION OF IMPENETRABLE CYLINDERS

ϕ_2	0.0	0.10	0.20	0.30	0.40	0.50	0.55	0.60	0.65
ζ_2	0.0	0.032	0.063	0.092	0.121	0.165	0.194	0.251	0.372

Before comparing our results for ζ_2 to other calculations, it is useful to obtain the low-density expansion of $I[\hat{S}_3]$ or ζ_2. To do so, we require the low-density expansion of the total correlation function $h(r)$. Through order ρ, we exactly have (Hansen & McDonald 1976) that

$$h(r) = \begin{cases} -1, & r < 1 \\ \rho A_2^{\text{int}}(r), & r > 1, \end{cases} \tag{4.11}$$

where

$$A_2^{\text{int}}(r) = [\pi - 2\arcsin(\tfrac{1}{2}r) - r(1-\tfrac{1}{4}r^2)^{\frac{1}{2}}]H(2-r) \tag{4.12}$$

is the intersection area of two discs of unit radius whose centres are separated by distance r. Substitution of (4.11) into (4.2) yields

$$k_2 = \tfrac{1}{6}\pi + 0.4107\,\phi_2 + O(\phi_2^2). \tag{4.13}$$

Because k_3 is multiplied by an additional factor ϕ_2, we need only substitute the zero-density limit of the total correlation function (i.e. $h(r) = -H(1-r)$] into (4.3) to obtain

$$k_3 = -1.024 + O(\phi_2). \tag{4.14}$$

Note that because the superposition approximation for g_3 is exact in the limit $\rho \to 0$, (4.14) is exact (within the accuracy of the numerical quadrature technique). Therefore, use of (3.41), (4.10), (4.13) and (4.14) leads to

$$\zeta_2 = \tfrac{1}{3}\phi_2 - 0.057\,07\,\phi_2^2 + O(\phi_2^3). \tag{4.15}$$

Equation (4.15) involves no approximation and hence is exact through order ϕ_2^2. The first-order coefficient of (4.15) depends upon $g_0(r)$, the zero-density limit of $g(r)$. The second-order coefficient of (4.16) depends on $g(r)$ through order ρ and on the zero-density limit of the triplet distribution function $g_3(r, s, t) = g_0(r)\, g_0(s)\, g_0(t)$. The aforementioned statements regarding the dependence of the first-order and second-order coefficients on g and g_3 apply generally to any distribution of discs (e.g. fully penetrable discs, discs with size distributions, etc.). Interestingly, the low-density expansion (4.15) provides a relatively good approximation of our calculations of ζ_2 through all orders in ϕ_2 (table 1) for the range $0 \leqslant \phi_2 \leqslant 0.4$.

In figure 1, the three-point parameter ζ_2 computed here is compared with the relatively few calculations of ζ_2 for other microstructures. This includes the symmetric-cell material (SCM) with cylindrical cells (Beran & Silnutzer 1971) for which $\zeta_2 = \phi_2$, square and hexagonal arrays of cylinders (McPhedran & Milton 1981) up to ϕ_2 very near their respective close-packing volume fraction, and fully penetrable cylinders (Torquato & Beasley 1986). Recall that the deviation of ζ_2 from 0 to 1 is a measure of the microstructural differences between the model of interest and the singly coated CCA geometries in which phase 2 and phase 1 are the dispersed phases, respectively.

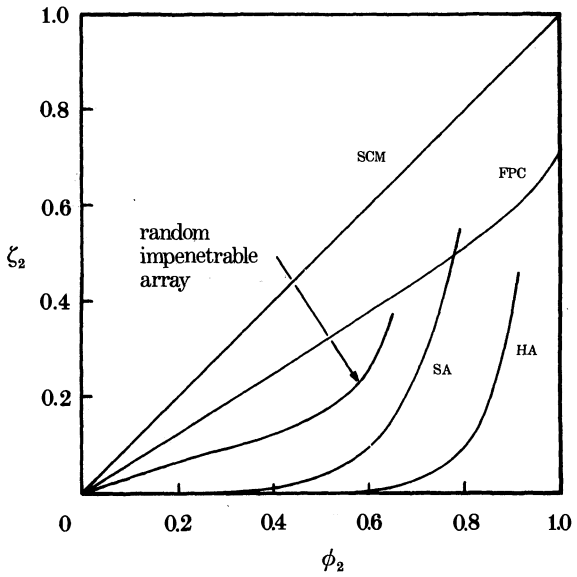

FIGURE 1. Three-point parameter ζ_2 for arrays of cylinders, including the symmetric-cell material (SCM), fully penetrable cylinders (FPC), square array (SA), hexagonal array (HA), and the random impenetrable array computed in this study.

Note that for all the models shown in figure 1, ζ_2 is a monotonically increasing function of ϕ_2 with $\zeta_2(\phi_2 = 0) = 0$. For general distributions, $\zeta_2(\phi_2 = 0)$ depends only upon the shape of the inclusion and hence is independent of the size distribution.

As remarked earlier, the slope of ζ_2 at $\phi_2 = 0$, $\zeta_2'(\phi_2 = 0)$, for general distributions

of inclusions, depends not only upon the shape of the inclusion but upon $g_0(r)$, the zero-density limit of the radial distribution function. The effect of size distribution of the inclusions, therefore, will be reflected in $\zeta_2'(\phi_2 = 0)$. For the equisized impenetrable-cylinder models depicted in figure 1 (square and hexagonal arrays and the random array), $\zeta_2'(\phi_2 = 0)$ is determined by integral (3.38) (or, equivalently, (4.2)). For random arrays of cylinders, the impenetrability constraint prohibits two centres from being closer than a diameter ($g_0(r) = 0$, $r < 1$) but for separations greater than a diameter ($2R$), the second cylinder relative to the first occupies all positions with equal probability ($g_0(r) = 1$, $r > 1$). This $g_0(r)$ leads to $\zeta_2'(\phi_2 = 0) = \frac{1}{3}$ as we have seen (cf. (4.15)). On the other hand, for regular arrays, $g_0(r) = 0$ for r less than distances of the order of $R\phi_2^{-\frac{1}{2}}$ and unity otherwise. Because $R\phi_2^{-\frac{1}{2}} \gg 1$ at dilute conditions, the form of the integrand of (3.38) implies that k_2 and thus $\zeta_2'(\phi_2 = 0)$ are zero. Thus, because periodic systems are 'well separated' for $\phi_2 \ll 1$, the expansion of ζ_2 through first order in ϕ_2 for these models is equal to that of the singly coated CCA model ($\zeta_2 = 0$) in which phase 2 is dispersed. In the case of fully penetrable discs, we have exactly that $g(r) = 1$ for all r, i.e. the cylinder centres are randomly centred and thus completely uncorrelated. For this model, integral (3.38) (which accounts for cylinder separations greater than 1) as well as integrals involving $g(r)$ for $r < 1$ (Torquato 1985*b*) contribute to $\zeta_2'(\phi_2 = 0)$. The latter contribution is positive, implying that $\zeta_2'(\phi_2 = 0)$ for this model must be greater than $\zeta_2'(\phi_2 = 0)$ for random rigid cylinders which is determined by (3.38) only. In the former case, $\zeta_2'(\phi_2 = 0) \approx 0.615$. Finally, although both the SCM and distributions of fully penetrable inclusions are models characterized by a high degree of 'randomness', the former, unlike the latter, is composed of cylindrical cells with a distribution of sizes such that they are space filling. This difference will be reflected in the $g_0(r)$ for these two models and presumably is the reason why $\zeta_2'(\phi_2 = 0)$ for the SCM is larger than the corresponding slope for fully penetrable cylinders.

It is noteworthy that ζ_2 for the SCM is exactly linear in ϕ_2 ($\zeta_2 = \phi_2$, Milton 1982) and hence is completely determined by the zero-density limit of the radial distribution function. Interestingly, for the case of fully penetrable cylinders, ζ_2 is nearly linear over the entire range of ϕ_2 and thus $\zeta_2'(\phi_2 = 0)$ is the dominant term in the expansion. The aforementioned similarities between the two models should not lead one to conclude that they are, in some rough sense, topologically similar. In fact, topologically they are strikingly different. Whereas the SCM exhibits topological equivalence, fully penetrable cylinders do not. (In cases where the morphology of phase 1 at volume fraction ϕ_1 is identical to that of phase 2 when the volume fraction of phase 1 is $1-\phi_1$, the composite is said to possess topological equivalence.) Unlike regular arrays of cylinders, ζ_2 for random impenetrable cylinders is approximately linear for the range $0 \leqslant \phi_2 \leqslant 0.4$. For random and periodic impenetrable cylinders, ζ_2 sharply rises as ϕ_2 approaches its respective close-packing value ϕ_2^c and apparently takes on its maximum value at ϕ_2^c. Exclusion-volume effects present in such models causes ζ_2 to sharply increase as ϕ_2^c. This is to be contrasted with the approximately linear behaviour of ζ_2 for the case of fully penetrable cylinders in which exclusion-volume effects are totally absent. For this model, ζ_2 is not characterized by any marked change in its

behaviour at the percolation threshold $\phi_2^c \approx 0.68$ (Gawlinski & Stanley 1981), which occurs well below $\phi_2 = 1$, i.e. the volume fraction at which ζ_2 is a maximum.

What is the significance of the precipitous increase of ζ_2 for square arrays over and above the values of the corresponding parameter for fully penetrable cylinders in the range $\phi_2 \geqslant 0.775$? To answer this question, we first examine the behaviour of the ζ_2 for these models for ϕ_2 less than the smaller of the two percolation thresholds, i.e. for $\phi_2 < 0.68$, where $\phi_2^c = 0.68$ is the critical value for fully penetrable cylinders (Gawlinski & Stanley 1981). For such ϕ_2, ζ_2 for penetrable inclusions is always greater than ζ_2 for the square array. Based upon the discussions in §2, this implies, for highly conducting inclusions ($\alpha \gg 1$), that fourth-order lower bound on σ_e (the bound that gives the good estimate of σ_e provided that $\Lambda_2 \ll L$) for the former will be above the one for the latter. This is fully consistent with our intuition that the effective conductivity of a system in which the inclusions may cluster must be larger than the σ_e of a system in which the inclusions are never in contact with one another. As soon as we cross the threshold for the overlapping case ($\phi_2 > 0.68$), then the fourth-order upper bound on σ_e will yield the useful estimate of the property for $\alpha \gg 1$. For the range $0.775 < \phi_2 < \frac{1}{4}\pi$ ($\phi_2^c = \frac{1}{4}\pi$ for the square array), ζ_2 for the periodic system is always greater than ζ_2 for overlapping cylinders. Hence, the fourth-order lower bound for the former will be above the one for the latter, given $\alpha \gg 1$. This does not mean that the lower bounds are incorrectly implying that σ_e for square arrays is larger than σ_e for fully penetrable cylinders: a system above its threshold. On the contrary, because the former is below its threshold, the fourth-order lower bound gives the estimate of σ_e, which clearly is below the estimate of σ_e for the fully penetrable case (i.e. the fourth-order upper bound).

Finally, we would like to note the interesting observation that $\zeta_2 = \phi_2$ for the SCM provides an upper bound on ζ_2 for all of the models described in figure 1, Placement of bounds on the parameter ζ_2 for any distribution of circular cylinders would be of great value, however, we cannot presently derive such bounds.

5. Evaluation of third-order and fourth-order bounds on σ_e

Using the results of the previous section for the microstructural parameter ζ_2, we evaluate the third-order bounds (2.1) and fourth-order bounds (2.7) for a random array of cylinders in a matrix. In figure 2 we plot the third-order and fourth-order bounds on the scaled conductivity σ_e/σ_1 as a function of the cylinder volume fraction for $\alpha = 10$. We include in this figure the corresponding second-order bounds due to Hashin. Note that the third-order and fourth-order upper bounds, rather than the corresponding lower bounds, provide most of the improvement relative to the second-order upper bound, as expected. The third-order bounds significantly improve upon the second-order bounds; the fourth-order bounds, in turn, are more restrictive than the third-order bounds. At $\phi_2 = 0.5$, the third-order bounds are about 3.7 times narrower than the Hashin bounds, whereas the fourth-order bounds are about 2.1 times narrower than the third-order bounds. For the range $0.1 \leqslant \alpha \leqslant 10$, the Milton bounds are sharp enough to

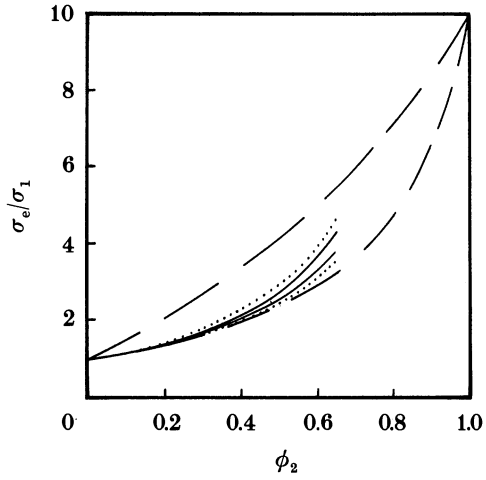

FIGURE 2. Bounds on σ_e/σ_1 as function of ϕ_2 at $\alpha = 10$. ---, Hashin bounds, ..., Silnutzer bounds; ——, Milton bounds for a random array of impenetrable cylinders.

give a good estimate of σ_e/σ_1 for the entire range of volume fractions reported. (For the case $\alpha = 0.1$ – not shown here – the Silnutzer and Milton bounds provide similar improvement over the Hashin bounds, except that most of the improvement is in the lower bound.)

In figure 3 we plot all three bounds on σ_e/σ_1 as a function of ϕ_2 for $\alpha = 100$. All the bounds, as expected, widen. At $\phi_2 = 0.5$, the Silnutzer bounds are about a factor of 2.8 narrower than the Hashin bounds; the Milton bounds are about a factor of 1.7 narrower than the Silnutzer bounds and hence are almost 5 times more restrictive than the Hashin bounds. For the range $0.01 \leqslant \alpha \leqslant 100$, the Milton bounds are sufficiently restrictive so as to give a good estimate of σ_e/σ_1 for the volume fraction range $0 \leqslant \phi_2 \leqslant 0.4$.

The fact that the bounds diverge as α is made larger does not mean that they cannot be used to estimate σ_e. As discussed in §2, because ϕ_2 is below the percolation point ($\phi_2^c \approx 0.81$) for randomly distributed rigid cylinders and because there are no particle contacts ($\Lambda_2 \ll L$), the lower bound should give a relatively good estimate of σ_e for $\alpha \gg 1$.

In figure 4 we plot all three lower bounds for the extreme case $\alpha = \infty$, i.e. perfectly conducting cylinders (the instance in which all upper bounds diverge to infinity). Milton's fourth-order lower bound is expected to yield a good estimate of σ_e, with the maximum error occurring at the maximum volume fraction reported here, i.e. at $\phi_2 = 0.65$ or $\phi_2/\phi_2^c \approx 0.80$. We can estimate the maximum error by comparing the Milton lower bound (2.9) for square and hexagonal arrays (McPhedran & Milton 1981) at $\phi_2/\phi_2^c = 0.80$ and for $\alpha = \infty$ to the exact results of Perrins *et al.* (1979). For square arrays, $\sigma_L^{(4)}/\sigma = 4.89$, whereas the exact result for $\sigma_e/\sigma_1 = 4.93$. For hexagonal arrays, $\sigma_L^{(4)}/\sigma_1 = 6.51$, whereas the exact result for $\sigma_e/\sigma_1 = 6.53$. Therefore, the maximum error in using Milton's lower bound to estimate the conductivity of a random array of perfectly conducting cylinders is expected to be about 1 % for $0 \leqslant \phi_2 \leqslant 0.65$. For values of α in the range $1 \leqslant \alpha < \infty$,

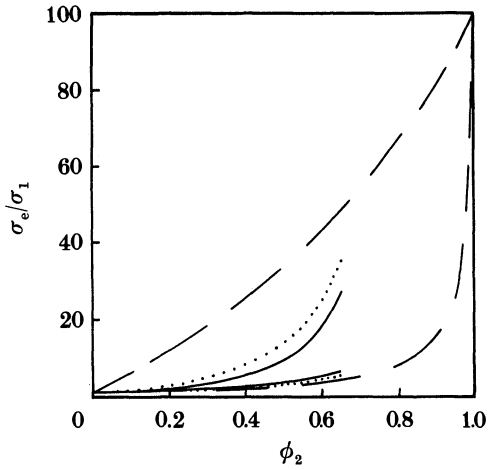

FIGURE 3. As figure 2, with $\alpha = 100$.

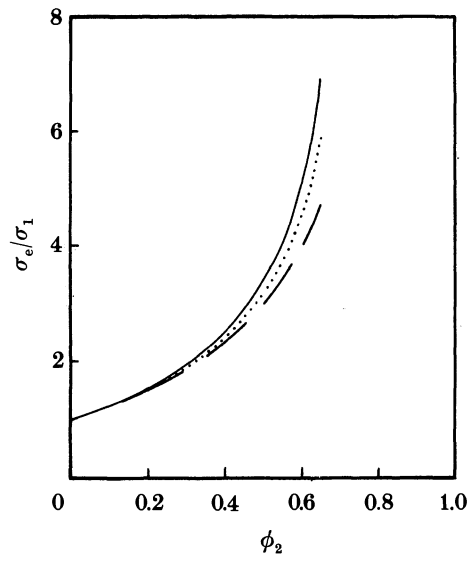

FIGURE 4. As figure 2, with $\alpha = \infty$. Upper bounds do not appear because they diverge to infinity in the limit $\alpha \to \infty$. Milton's fourth-order lower bound, however, gives an excellent estimate of σ_e/σ_1.

the deviation of Milton's lower bound from exact results is even less than it is for $\alpha = \infty$. In short, the fourth-order lower bound on σ_e provides an excellent estimate of this quantity for random arrays of cylinders for the entire volume-fraction range studied here, even when the cylinders are infinitely conducting.

S.T. gratefully acknowledges support of the Office of Basic Energy Sciences, U.S. Department of Energy, under Grant No. DEFG05-86ER13482. F.L. acknowledges the support of the National Science Foundation under Grant No. CHE-84-02144. We thank J. D. Beasley, P. A. Smith and A. K. Sen for very useful discussions.

Appendix A. Alternative representation of expansion coefficients

Consider some function $f(t)$ which depends only on the magnitude t of the vector $\boldsymbol{t}$. The orthogonality of the Chebyshev polynomials yields the inverse of the expansion

$$f(t) = \sum_{n=0}^{\infty} F_n(r,s)\, T_n(\cos\theta) \tag{A 1}$$

as

$$F_n(r,s) = \frac{c_n}{2\pi} \int \mathrm{d}\theta f(t)\, T_n(\cos\theta), \tag{A 2}$$

where the c_n are given by (3.10) and $t^2 = r^2 + s^2 - 2rs\cos\theta$. Now suppose that $f(t)$ possesses a Fourier transform $\tilde{f}(k)$, so that

$$f(t) = \frac{1}{4\pi^2} \int \mathrm{d}\boldsymbol{k} \tilde{f}(k) \exp(\mathrm{i}\boldsymbol{k}\cdot\boldsymbol{t}). \tag{A 3}$$

Here k is the magnitude of the wavenumber vector $\boldsymbol{k}$ and $\mathrm{i} = \sqrt{-1}$. We now show that (A 2) can alternatively be written in terms of the transform $\tilde{f}(k)$. Arrange the coordinate frame such that the vector $\boldsymbol{r}$ emanates from the origin and lies along the x-axis; in this frame, let ϕ be the angular coordinate of $\boldsymbol{k}$. Letting $\beta = \theta - \phi$, we then have

$$\begin{aligned}
\exp(\mathrm{i}\boldsymbol{k}\cdot\boldsymbol{t}) &= \exp[\mathrm{i}\boldsymbol{k}\cdot(\boldsymbol{s}-\boldsymbol{r})] = \exp[\mathrm{i}ks\cos\beta]\exp(-\mathrm{i}kr\cos\phi) \\
&= \Bigg[J_0(ks) + 2\sum_{m=1}^{\infty}(-1)^m J_{2m}(ks)\cos 2m\beta \\
&\quad + 2\mathrm{i}\sum_{m=0}^{\infty}(-1)^m J_{2m+1}(ks)\cos(2m+1)\beta\Bigg] \\
&\quad \times\Bigg[J_0(kr) + 2\sum_{n=1}^{\infty}(-1)^n J_{2n}(kr)\cos 2n\phi \\
&\quad - 2\mathrm{i}\sum_{n=0}^{\infty}(-1)^n J_{2n+1}(kr)\cos(2n+1)\phi\Bigg],
\end{aligned} \tag{A 4}$$

where, using the generating function for the Bessel function J_n (Abramowitz & Stegun 1964), we have expanded plane waves in cylindrical waves. Substitution of (A 4) into (A 3) then leads to

$$f(t) = \frac{1}{2\pi}\int_0^{\infty} \mathrm{d}k\, k\tilde{f}(k) \sum_{n=0}^{\infty} c_n J_n(kr) J_n(ks) T_n(\cos\theta). \tag{A 5}$$

Comparing (A 5) with (A 1) gives

$$F_n(r,s) = \frac{c_n}{2\pi}\int_0^{\infty} \mathrm{d}k\, k\tilde{f}(k) J_n(kr) J_n(ks), \tag{A 6}$$

which is sometimes a convenient alternative to (A 2).

Appendix B. Some useful identities

Here we shall prove the following relations for the triangle with sides of length r, s, and t:

$$\left(\frac{r}{t}\right)^2 \cos 2\phi = \left(\frac{r}{t}\right)^2 T_2(\cos\phi) = \sum_{n=0}^{\infty} (n+1)\left(\frac{s}{r}\right)^n T_{n+2}(x), \tag{B 1}$$

$$\left(\frac{r}{t}\right)^2 \sin 2\phi = \left(\frac{r}{t}\right)^2 V_2(\cos\phi) = \sum_{n=0}^{\infty} (n+1)\left(\frac{s}{r}\right)^n V_{n+2}(x). \tag{B 2}$$

Here ϕ and θ are the angles opposite the sides of length r and t, respectively; $x = \cos\theta$, $T_n(x) = \cos n\theta$ is the Chebyshev polynomial of the first kind, and $V_n(x) = \sin n\theta$ is a polynomial related to the Chebyshev polynomial $U_n(x)$ of the second kind defined below.

The Chebyshev polynomial of the second kind is defined through the generating function

$$\left(\frac{r}{t}\right)^2 = \frac{1}{1+(s/r)^2-2(s/r)x} = \sum_{n=0}^{\infty}\left(\frac{s}{r}\right)^n U_n(x). \tag{B 3}$$

Differentiating (B 3) with respect to x gives

$$\left(\frac{r}{t}\right)^4 = \frac{1}{2}\sum_{n=1}^{\infty}\left(\frac{s}{r}\right)^{n-1} U_n'(x), \tag{B 4}$$

where the prime denotes the first derivative. Now

$$\cos 2\phi = 1-2(r/t)^2\sin^2\theta \tag{B 5}$$

and hence

$$\left(\frac{r}{t}\right)^2 \cos 2\phi = \sum_{n=0}^{\infty}\left(\frac{s}{r}\right)^n [U_n(x)-(1-x^2)U_{n+1}'(x)]$$

$$= \sum_{n=0}^{\infty}(n+1)\left(\frac{s}{r}\right)^n T_{n+2}(x), \tag{B 6}$$

which is one of the relations we set out to prove. The second line of (B 6) follows from recurrence relations for Chebyshev polynomials (Abramowitz & Stegun 1964).

The use of the identity

$$(r/t)^2 \sin 2\phi = 2(r/t)^4 (x-s/r)\sqrt{(1-x^2)} \tag{B 7}$$

in conjunction with (B 4) yields

$$\left(\frac{r}{t}\right)^2 \sin 2\phi = \sum_{n=0}^{\infty}\left(\frac{s}{r}\right)^n \sqrt{(1-x^2)}\,[xU_{n+1}'(x)-U_n'(x)]$$

$$= \sum_{n=0}^{\infty}(n+1)\left(\frac{s}{r}\right)^n V_{n+2}(x), \tag{B 8}$$

where

$$V_{n+1}(x) = \sqrt{(1-x^2)}\,U_n(x). \tag{B 9}$$

This proves (B 2). Again, the second line of (B 8) follows from recursion relations.

References

Abramowitz, M. & Stegun, I. A. 1964 *Handbook of mathematical functions*. Washington, D.C.: National Bureau of Standards.
Beasley, J. D. & Torquato, S. 1986 *J. appl. Phys.* **60**, 3576–3581.
Beran, M. & Silnutzer, N. 1971 *J. composite Mater.* **5**, 246–249.
Brown, W. F. 1955 *J. chem. Phys.* **23**, 1514–1517.
Feder, J. 1980 *J. Theor. Biol.* **87**, 237–254.
Gawlinski, E. T. & Stanley, H. E. 1981 *J. Phys.* A **14**, L291–L299.
Hansen, J. P. & McDonald, I. R. 1976 *Theory of simple liquids*. New York: Academic Press.
Hashin, Z. 1970 In *Mechanics of composite materials* (ed. F. W. Wendt, H. Liebowitz & N. Perrone), pp. 201–242. New York: Pergamon Press.
Joslin, C. G. & Stell, G. 1986 *J. appl. Phys.* **60**, 1607–1610.
Lado, F. 1968 *J. chem. Phys.* **49**, 3092–3096.
McPhedran, R. F. & Milton, G. W. 1981 *Appl. Phys.* A **26**, 207–220.
Miller, M. 1969 *J. math. Phys.* **10**, 1988–2004.
Milton, G. W. 1981 *J. appl. Phys.* **52**, 5294–5304.
Milton, G. W. 1982 *J. Mech. Phys. Solids* **30**, 177–191.
Phan-Thien, N. & Milton, G. W. 1982 *Proc. R. Soc. Lond.* A **380**, 332–348.
Perrins, W. T., McKenzie, D. R. & McPhedran, R. C. 1979 *Proc. R. Soc. Lond.* A **369**, 207–225.
Silnutzer, N. 1972 Ph.D. Thesis, University of Pennsylvania, Philadelphia.
Stillinger, F. H., DiMarzo, E. A. & Kornegay, R. L. 1964 *J. chem. Phys.* **40**, 1564–1576.
Torquato, S. 1985*a* *J. appl. Phys.* **58**, 3790–3797.
Torquato, S. 1985*b* *J. chem. Phys.* **83**, 4776–4785.
Torquato, S. & Beasley, J. D. 1986 *Int. J. engng Sci.* **24**, 415–433.
Torquato, S. & Stell, G. 1982 *J. chem. Phys.* **77**, 2071–2077.
Torquato, S. & Stell, G. 1985 *J. chem. Phys.* **82**, 980–987.

Note added in proof (26 *January* 1988). Durand & Ungar have very recently written a paper (to be published in the *International Journal of Numerical Methods in Engineering* in which they use a computer simulation procedure to exactly, within numerical error, determine the effective conductivity, for the same equilibrium cylinder model studied here, for $\alpha = 50$ at three volume-fraction values, $\phi_2 = 0.2$, 0.4 and 0.6. The fourth-order lower bound (2.9), computed in this study, predicts conductivities which are virtually identical to the ones obtained by Durand & Ungar. This supports our comments that bounds (which are relatively inexpensive to compute) can be used to accurately estimate σ_e, even when the phase properties widely differ. Moreover, this strongly indicates that the use of the superposition approximation (4.1) to calculate (3.39) does not lead to significant errors in the microstructural parameter ζ_2.